Diamond & Related Materials xxx (xxxx) 110362

Contents lists available at ScienceDirect

Diamond & Related Materials

journal homepage: www.elsevier.com/locate/diamond

Graphene on SiO_2/Si and Al_2O_3 under thermal annealing and electric current: Competition of dopant desorption and conformation to substrate

E.A. Kolesov [a,*], M.S. Tivanov [a], O.V. Korolik [a], I.A. Svito [a], A.S. Antonovich [a], Yu. Klishin [b], D.A. Ghazaryan [b,c], A.V. Arsenin [b,c], V.S. Volkov [b,c], O.O. Kapitanova [b,d], G.N. Panin [e]

[a] Belarusian State University, Nezavisimosti av. 4, 220030 Minsk, Belarus
[b] Center for Photonics and 2D Materials, Moscow Institute of Physics and Technology, 9 Institutskiy per., 141701 Dolgoprudny, Moscow Region, Russia
[c] Laboratory of Advanced Functional Materials, Yerevan State University, 1 Alek Manukyan, Yerevan 0025, Armenia
[d] Faculty of Chemistry, Moscow State University, 1 Leninskie Gory, 119991 Moscow, Russia
[e] Institute of Microelectronics Technology and High-Purity Materials of RAS, Institutskaya, 6, 142432 Chernogolovka, Russia

ARTICLE INFO

Keywords:
Graphene
Raman spectroscopy
Current-voltage characteristic
Annealing
Adsorption
Conformality

ABSTRACT

In this work, we study phonon and electronic properties of graphene on SiO_2/Si and Al_2O_3 by simultaneous Raman and electrical measurements in the temperature range from room temperature to 550 °C, or at voltages from 20 to −20 V. The dependencies of G and 2D peak parameters and electrical resistance on temperature and voltage made it possible to observe *in situ* a competition between the *p*-type adsorbate removal from graphene surface and substrate-induced doping due to graphene-substrate conformality increase, both stimulated by either ambient or Joule heating. The analyzed parameters were dominated by the conformality increase, with the hole density increasing significantly and unidirectionally, while resistance and I-V curves fluctuated due to the competition. Having calculated Raman peak shift temperature coefficients, resistance temperature coefficients, total variations of carrier density, resistance and strain, we show that Al_2O_3 substrate can be used to reduce the desorption barrier, the overall doping, the impact on graphene resistance and on phonon anharmonicity – however, it should be used with regard to the possibility of introducing strain or stronger doping after longer treatments. The conformality effects should be taken into account when performing annealing, as well as graphene applications for sensors or strong electric currents.

1. Introduction

Graphene became popular due to its exceptional properties, including high values of thermal [1] and electrical [2] conductivity, carrier mobility and magnetoresistance [3], mechanical stiffness [1], as well as strong sensitivity to adsorbates [4–13]. In particular, atmospheric adsorption on air-exposed graphene leads to integral *p*-type doping due to the acceptor H_2O and O_2 adsorbates [4,6–9,13,14]. This effect can be unwanted if graphene-air interface is present; on the other hand, strong graphene adsorptivity can be used as a constituent part of the methods for graphene functionalization through the adsorption of certain functional groups, for chemical and environmental sensors, selective catalysis and other applications [6–14].

Removal of adsorbates is traditionally made by annealing; it also can be performed by passing electric current (integrally – through the Joule heating) [15] or by laser annealing (locally) [13,14]. At the same time, when graphene is integrally annealed, its adherence to the substrate becomes stronger [6,16–21]; its properties, which are in principle affected by the degree of graphene-substrate conformality [21], correspondingly change. Therefore, studying the adsorption doping of similar samples of graphene supported by different substrates, pristine or integrally annealed either traditionally (ambient heating) or by passing electric current within a single series of experiments will not only clarify the relationship between the influence of substrate and adsorption doping on carrier density in graphene, but also enable one to control the properties of the material by choosing the substrate type to achieve desired results, depending on the annealing temperatures or considering a certain degree of conformality, *etc.*

While SiO_2/Si is a typical substrate associated with graphene, Al_2O_3 is another promising dielectric surface for supporting this material, capable of affecting graphene properties less than the former at least by criteria of phonon scattering and doping by atmospheric adsorbates. In particular, Al_2O_3 substrate was shown to induce less phonon anharmonicity in graphene during the low-temperature experiments, show-

* Corresponding author.
E-mail address: kolesov.bsu@gmail.com (E.A. Kolesov).

https://doi.org/10.1016/j.diamond.2023.110362
Received 20 July 2023; Received in revised form 29 August 2023; Accepted 31 August 2023
0925-9635/

ing the anharmonic constant values close to those for unsupported graphene [22]. Besides, graphene supported by Al_2O_3 was demonstrated to lose acceptor adsorbates more easily when placed in vacuum [23]. Given the close graphene-substrate interaction energy values of 0.45 J/m² against 0.47 J/m² for SiO_2/Si and Al_2O_3, respectively [24,25], these two are suitable for comparative study in the context of the substrate-related effects.

Raman spectroscopy is a well-known and versatile non-destructive method to obtain information about the properties of graphene [26,27]. At the same time, current-voltage (I-V) characteristic measurement is a basic way to get the data essential for analysis of the electric properties of materials, which in the case of two-dimensional graphene will be naturally affected by the presence of dopant adsorbates.

The purpose of this work is to establish phonon and electronic properties of graphene on SiO_2/Si and Al_2O_3 by Raman spectroscopy with parallel direct-current electrical resistance measurements in the temperature range from room to 550 °C, or with parallel I-V characteristic measurements under voltages from 20 to −20 V.

2. Experimental

Graphene was synthesized by chemical vapor deposition on an Alfa Aesar copper foil substrate with a purity of 99.999 %, a thickness of 25 μm and an area of 10 × 30 cm² at a temperature of 1020 °C with CH_4 flow of 40 sccm and hydrogen flow of 10 sccm. The substrate prepared for synthesis was treated by the preliminary annealing at a temperature of 1060 °C for 1 h under the flow of hydrogen of 300 sccm and argon of 2000 sccm, with a base pressure of $<10^{-4}$ Torr. After the synthesis, graphene was transferred to SiO_2/Si and Al_2O_3(0001) substrates using PMMA [28]. PMMA with a molecular weight of 996,000 g/mol, dissolved in anisole, was spin-coated (3000 rpm, 1 min) on graphene supported by copper foil. Then, an aqueous solution of 0.1 M $(NH_4)_2S_2O_8$ was utilized for copper etching; the etching products were removed from graphene using a water/isopropyl alcohol mixture [29]. To remove the PMMA, the sample was kept in extra-pure glacial acetic acid [30] for 24 h.

The SiO_2 layer thickness in a SiO_2/Si substrate prepared for graphene transfer was of 90 nm (over a 500 μm Si wafer). SiO_2/Si and Al_2O_3(0001) substrates were atomically smooth, which according to preliminary AFM evaluations corresponded to the roughness below ~0.5 nm (RMS roughness below ~1.5 nm). Using photolithography, 60 nm Au contact pads with a 5 nm Cr sublayer for adhesion increase were fabricated on SiO_2/Si and Al_2O_3 (0001) substrates, prior to graphene transfer. These layers were deposited in a single mode by electron beam evaporation (NanoMaster NEE-4000). The contact configuration will be shown later as inset in Fig. 2.

Raman spectra were obtained using Nanofinder HE (Lotis-TII) confocal Raman spectrometer. The spectral resolution was of 2.3 cm^{-1} in the region of the G peak and 1.0 cm^{-1} in the region of the 2D peak, the total spectral resolution during the measurements was better than 3.0 cm^{-1}. The radiation was excited using a CW-laser with a wavelength of 532 nm. For measurements on air, the laser spot diameter was of 0.6 μm and radiation power at the output of the optical system was of 800 μW; for measurements in a pressure- and temperature-controlled chamber, the laser spot diameter was of 1.5 μm and radiation power was of 2.4 mW. This high value of radiation power was chosen manually and was used to compensate the attenuation by ~3.3 times due to chamber glass absorption and by ~10.8 times due to using a long focal length lens.

To analyze the electronic and phonon properties of graphene, Raman spectra were measured (1) on air; (2) in vacuum ($<5 \times 10^{-5}$ mbar); (3) in vacuum within the temperature range from room to 550 °C with simultaneous measurement of resistance at a direct current of 0.01–1.00 mA, in two cycles; (4) in vacuum with simultaneous I-V curve measurements in the range from 20 to −20 V, in two cycles. When measuring the I-V characteristics, each voltage value was maintained for 40 s, the Raman spectra were measured with an exposure of 30 s, the pauses between the spectra measurements were of 10 s.

3. Results and discussion

The Raman spectra of graphene on SiO_2/Si and Al_2O_3 substrates obtained in air and in vacuum ($<5 \times 10^{-5}$ mbar) are shown in Fig. 1. G and 2D peaks are typical for a hexagonal sp^2 carbon lattice; the presence of single-layer graphene is confirmed by the ratio of the 2D and G peak maximum intensities I_{2D}/I_G of at least 2.1, as well as the 2D peak full width at half-maximum (FWHM) ~ 28–35 cm^{-1} [26,27]. In all cases, the G peak position is of about 1586–1592 cm^{-1}, 2D – that of 2680–2685 cm^{-1}; at the same time, average peak position values over the scanned regions are generally larger for the case of the SiO_2/Si substrate, although they can differ by ±1–5 cm^{-1} from point to point. The positions of the peaks, initially increased by 4 to 9 cm^{-1} with respect to the isolated graphene typical values [26,27] and decreasing as the pressure decreases, are related to the presence of H_2O and O_2 acceptor adsorbates on the surface of graphene, that desorb when air is removed from the measuring cell [4–9,13,14]. Charge carrier density change can be calculated based on the dependencies presented in [31] from G and 2D peaks shift (due to various laser excitation wavelengths in the cited literature, the dispersion correction [26] was accordingly taken into ac-

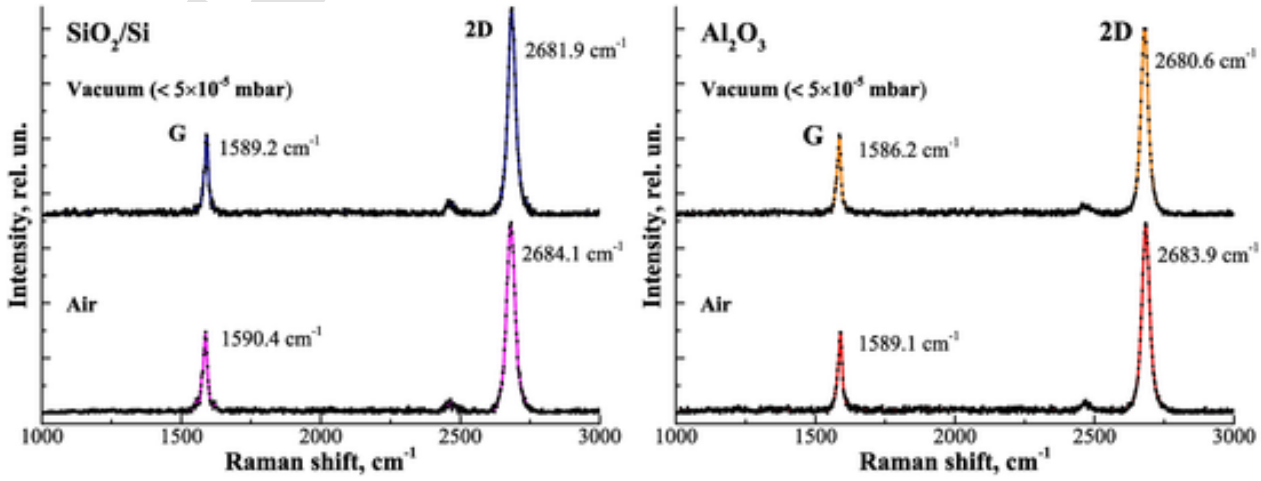

Fig. 1. Typical Raman spectra of graphene on SiO_2/Si and Al_2O_3 in air and in vacuum ($<5 \times 10^{-5}$ mbar).

count for all calculations involving 2D peak position throughout this work). In the case of the SiO_2/Si substrate, excess hole density changes from 4.7 × 10^{12} cm^{-2} to 2.9 × 10^{12} cm^{-2} (Fermi level E_F shift from ~−278 meV to ~−218 meV below the Dirac point), for graphene on Al_2O_3 the decrease is from 4.5 × 10^{12} cm^{-2} to 2.1 × 10^{12} cm^{-2} (E_F change from ~−272 meV to ~−186 meV). The larger initial atmospheric doping of graphene on SiO_2/Si and the smaller hole density decrease in this case can be related to different electrostatic doping of graphene by different substrates [32].

Fig. 2 shows temperature dependencies for Raman features of graphene on SiO_2/Si and Al_2O_3, as well as its resistance at a direct current of 0.01–1.00 mA for two successive measurement cycles with indication of start and end points. The $FWHM_{G,2D}$ did not show any significant patterns. As can be seen from the figure, the behaviour of all dependencies at first heating differs from their subsequent shape (this can be basically called a 'primary annealing'). During the primary annealing process, peak positions ω_G and ω_{2D} have a smaller slope to the horizontal axis, and show a non-linear behaviour at temperatures above 400 °C, before switching to linear temperature dependence, which is in accordance with the literature data in this temperature range [1,33–42]. Over the following cooling-heating-cooling steps, the angle is larger, and the dependencies are repeatable. Linear coefficients for the primary annealing $\chi_{G,2D}{}^1$ and for subsequent temperature changes $\chi_{G,2D}$ are presented in Table 1, along with the corresponding intercepts for temperature close to absolute zero. No graphene structural degradation in terms of D peak emergence [26,27] was observed during the treatment. It should be strongly emphasised that ω^0 values obtained from a linear fit tend to be significantly overestimated [22], and are given here solely for a comparison purpose, in accordance with a tradition established within the field [1,33–42].

The ω^0 related changes in Table 1 are generally stronger for the case of Al_2O_3 substrate, which implies that its 'smaller' effect on graphene properties [22,23] is only maintained until a heat treatment is performed. At the same time, all χ absolute values are larger for graphene on SiO_2/Si. As the primary annealing occurs, the average increase of the peak temperature shift coefficient $\chi_G{}^1$-χ_G is of ~1.2 times for both substrate cases, while for $\chi_{2D}{}^1$-χ_{2D} it is of ~1.7 times. When comparing the values presented in Table 1 with those already published elsewhere, one cannot fail to notice that the literature data on linear fits of graphene Raman peak temperature shift generally allows to identify the results as those aligning with $\chi_G{}^1$ (−0.015 [35,36], −0.016 [37,38], −0.018 [22,39], −0.019 [40] cm^{-1}/K), when no temperature treatment or a single/first experiment have been performed, and those that are increased as a result of a primary annealing (−0.035 [41], −0.073 [39] cm^{-1}/K). There is somewhat less data presented for 2D peak, but some works show its temperature shift coefficient as having the pre-annealing value (−0.026 [42], −0.039 [36] cm^{-1}/K), or as the one increased due to several preliminary temperature treatments (−0.070 [41] cm^{-1}/K). This observation allows concluding that χ coefficient classifying into one of these groups basically enables to retroactively establish, if the annealing has been performed either by preliminary temperature treatment or by performing multiple experiments.

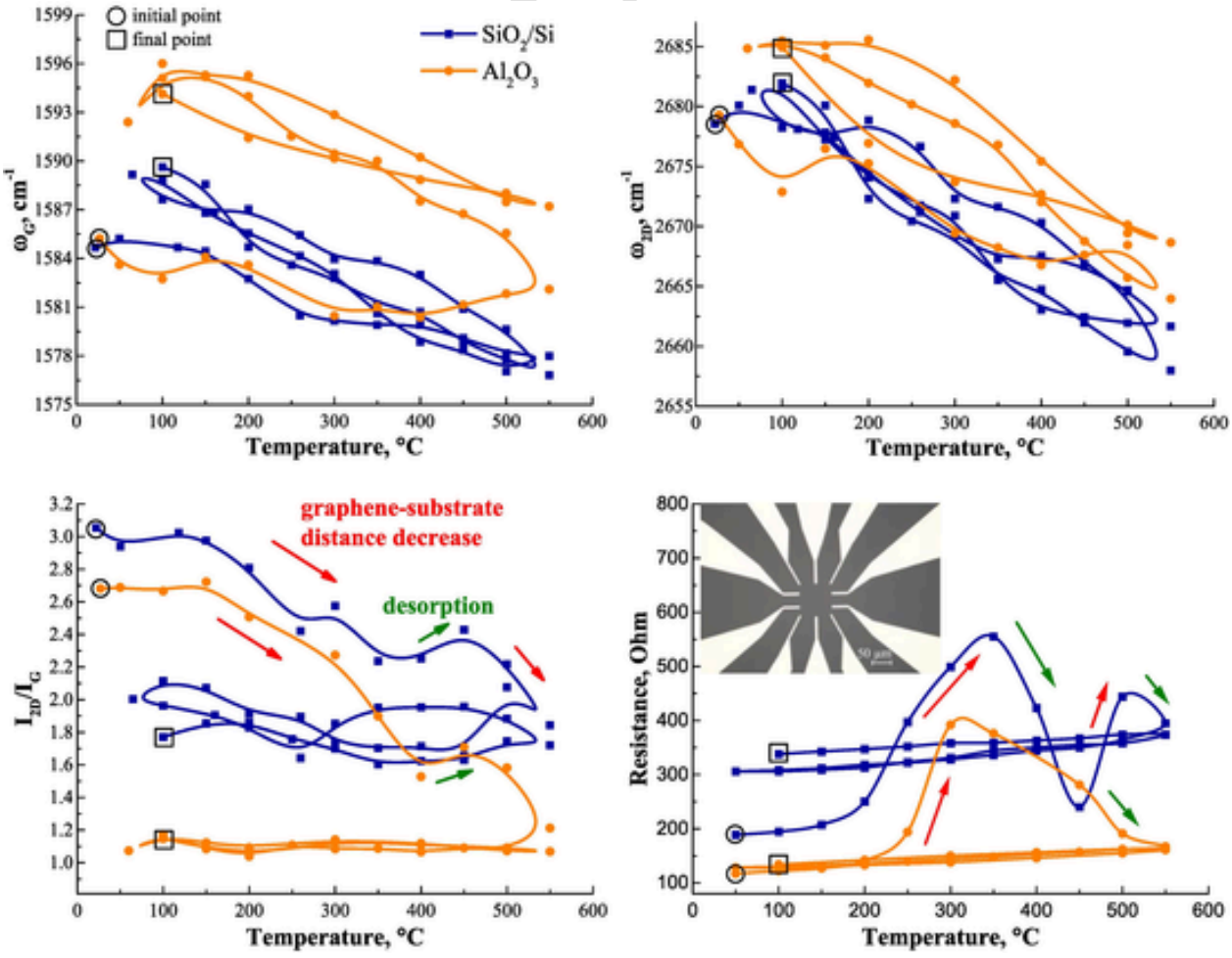

Fig. 2. Temperature dependencies of the G and 2D peak positions ω_G, ω_{2D}, the intensity ratio I_{2D}/I_G, as well as resistance at a direct current of 0.01–1.00 mA for graphene on SiO_2/Si and Al_2O_3, for two successive heating cycles. Inset shows optical image of the Al_2O_3(0001)/Cr/Au contacts.

Table 1
Linear coefficients of G and 2D peak position temperature dependencies $\chi_{G,2D}$ and resistance temperature dependencies α for graphene on SiO_2/Si and Al_2O_3 in the range from room temperature to 550 °C for the primary annealing (marked with digit *1*) and subsequent temperature changes, as well as corresponding intercepts for temperature close to absolute zero $\omega^0_{G,2D}$, R_0.

Substrate	SiO_2/Si		Al_2O_3	
$\omega^{0\ 1}_G$, cm^{-1}	1589.7	±0.8	1588.1	±1.2
ω^0_G, cm^{-1}	1598.3	±0.9	1603.0	±1.0
χ^1_G, cm^{-1}/K	−0.015	±0.001	−0.012	±0.002
χ_G, cm^{-1}/K	−0.026	±0.001	−0.021	±0.002
$\omega^{0\ 1}_{2D}$, cm^{-1}	2694.3	±1.8	2687.3	±2.5
ω^0_{2D}, cm^{-1}	2698.0	±1.9	2699.9	±2.1
χ^1_{2D}, cm^{-1}/K	−0.042	±0.003	−0.030	±0.005
χ_{2D}, cm^{-1}/K	−0.048	±0.003	−0.039	±0.004
dR/dT, Ω/K	0.134	±0.016	0.063	±0.006
R_0, Ω	263.4	±9.5	111.9	±3.6
α, K^{-1}	$5.1{\cdot}10^{-4}$	$\pm 0.8{\cdot}10^{-4}$	$5.6{\cdot}10^{-4}$	$\pm 0.6{\cdot}10^{-4}$

In addition to the data presented in Fig. 2 for ω_G, ω_{2D} temperature dependencies, a gradual decrease of the intensity ratio I_{2D}/I_G for graphene on both substrates is observed during the primary annealing; following that, I_{2D}/I_G remains approximately constant with subsequent changes in temperature. The excess hole density increase obtained from the complete I_{2D}/I_G change [31] during the treatment is $\Delta p \sim 3.3 \times 10^{12}$ cm^{-1} ($\Delta E_F \sim -127$ meV) for graphene on SiO_2/Si substrate, while the case of Al_2O_3 substrate brings a stronger Δp increase of about 6.1×10^{12} cm^{-1} ($\Delta E_F \sim -159$ meV). Simultaneously with the 2D-G intensity ratio evolution, changes in the resistance of graphene are observed as the temperature changes, and it should be noted that these dependencies in part inversely correspond to each other, while being obtained by different methods. As the heating starts, the resistance increases by 360.1 Ω for graphene on SiO_2/Si and by 269.7 Ω for graphene on Al_2O_3, reaching maxima at temperatures of 300–350 °C; then it tends to decrease after some fluctuations in case of the former substrate and more straightforwardly for the latter, resolving to a near-linear temperature dependence with parameters presented in Table 1. As seen from the table, the resistance-temperature derivative dR/dT for graphene on SiO_2/Si is almost double than that for Al_2O_3, while the reduced coefficient $\alpha = (dR/dT)/R_0$ values are close for the cases of both substrates, their values overlapping within the error.

The initial increase of the resistance, simultaneous with the excess hole density increase, for graphene under heating in vacuum clearly indicates that there is an acceptor source, other than the adsorbates getting removed by the temperature treatment and pumping (which would have reduced the resistance [7]). Among what is present in the vacuum chamber, the substrate remains as such source: with the energy provided during the annealing, graphene-substrate conformality is known to increase, effectively making a transition from quasi-suspended behaviour due to a non-zero substrate roughness to a strongly adhered configuration [20]. Through increasing the effective contact surface area, this enhances graphene-substrate charge transfer, which was reported as inducing Fermi level downshift to the *p*-type direction for both SiO_2/Si [43] and Al_2O_3 [44] substrates. The removal of water layer intercalated at the interface by temperature treatment [20,45–47] additionally enhances graphene-substrate Van der Waals interaction, leading to the assimilation of substrate topology by the 2D material and furtherly strengthening the charge transfer effect. The material-substrate conformation processes occur during the annealing simultaneously with the proceeding removal of adsorbates from the surface of graphene, leading to a competition of increasing/reducing the excess hole density, as well as the resistance. This leads to a complex shape of I_{2D}/I_G and R(T) primary annealing dependencies seen in Fig. 2, where the evidence of both effects is indicated by red and green arrows.

It is very much worth noting that I_{2D}/I_G(T), effectively manifesting charge carrier density through Fermi level shift, decreases irrevocably within the experiment, showing only vague desorption steps, while R (T) shows somewhat different sensitivity, as seen from full compensation of the two effects in case of Al_2O_3 substrate: after the first increase due to graphene-substrate conformation domination, the dependency decreases back to the initial range of values due to the desorption. This indicates that (1) in common, graphene-substrate conformation effects are explicitly manifested in the carrier density effects rather that resistance which can be an ambiguous evidence, but (2) in particular, the SiO_2/Si substrate does affect graphene resistance after the thermal treatment, unlike in the case of Al_2O_3.

Another method that can be used to analyze the effects of desorption and graphene-substrate conformation, observed in Fig. 2, is plotting the 2D-G peak position diagram [48,49], where one can distinguish separate directions for mechanical strain, hole and electron variations. Fig. 3 demonstrates the 2D-G diagram for graphene on Al_2O_3 and SiO_2/Si, with points corresponding to spectra obtained *at a room temperature before/between/after heating treatments* to avoid the influence of anharmonic effects and thermal expansion strain [22] on the peak position (1 – before the first heating cycle, 2 – between the first and second heating cycles, 3 – after the second heating cycle). The reference point corresponds to isolated graphene [26]. As can be seen from Fig. 3, a sharp excess hole density increase occurs in graphene after the first cycle (point 2) for the cases of both substrates, manifesting the domination of charge transfer from the substrate, while between points 2 and 3, the changes are less significant, which is in agreement with I_{2D}/I_G(T) dependence in Fig. 2, indicating either the termination of desorption/substrate conformation processes, or their mutual compensation. The total excess hole density increase obtained from the peak positions [31] is $\Delta p \sim 2.8 \times 10^{12}$ cm^{-2} ($\Delta E_F \sim -101$ meV) and $\Delta p \sim 5.2 \times 10^{13}$ cm^{-2} ($\Delta E_F \sim -146$ meV) for graphene on SiO_2/Si and Al_2O_3, respectively, which corresponds well to the values obtained earlier from I_{2D}/I_G change. The emergence of mechanical strain is not observed within the sensitivity of the method [50].

Fig. 4 shows the I-V curves obtained by passing an electric current through graphene in vacuum within the voltage range from 20 to −20 V in 2 cycles, as well as the corresponding changes in resistance. In the 1st I-V measurement cycle, the pronounced inflections (marked by circles) are observed, associated with an increase of electrical resistance to maximum values of 941.7 and 730.5 Ω at voltages of 14 and 18 V for graphene on SiO_2/Si and Al_2O_3, respectively (the second increase in the case of SiO_2/Si is up to 336.6 Ω at −16 V). As in the case of heat treatment, this indicates presence of competition between the graphene-substrate conformation and desorption stimulated by current/Joule heating, as indicated by red and green arrows on the resis-

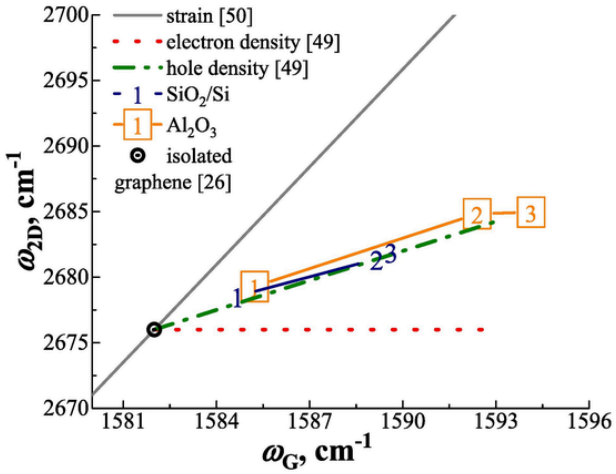

Fig. 3. 2D-G position diagram for graphene on SiO_2/Si and Al_2O_3 before, between and after two successive heating cycles to a temperature of 550 °C; reference point corresponds to isolated graphene.

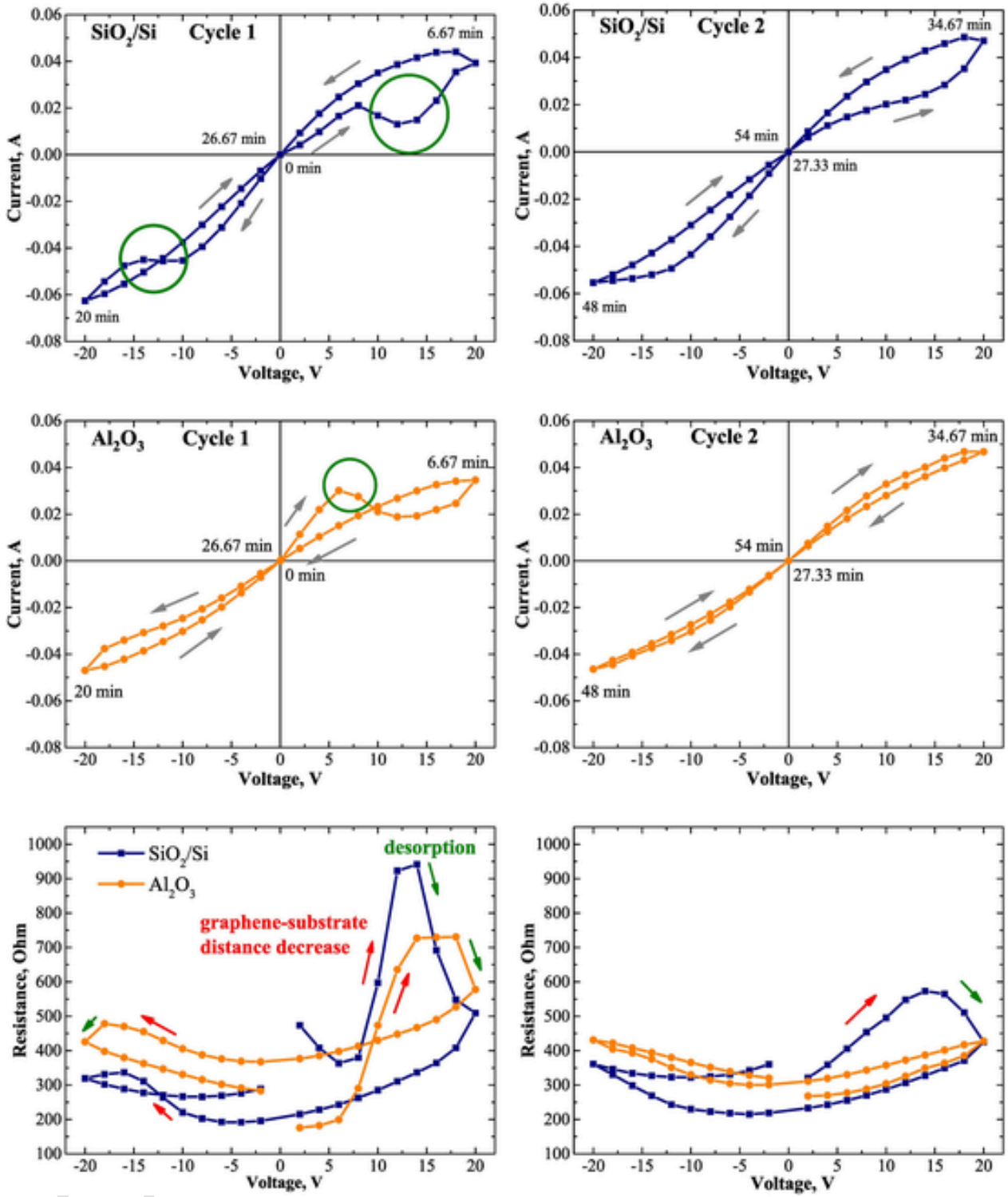

Fig. 4. I-V characteristics for graphene on SiO_2/Si and Al_2O_3 for two successive measurement cycles in the range from 20 to −20 V, with indicated time of the cycle beginning, the first voltage maximum (20 V), the second voltage maximum (−20 V), the end of the cycle; as well as the corresponding electrical resistance.

tance plots in Fig. 4. Generally, the resistance of graphene on SiO_2/Si decreases from 473.4 to 288.6 Ω after the 1st cycle (domination of desorption) and increases to 360.3 Ω at the end of the 2nd cycle (the following prevailing of conformation). For Al_2O_3 substrate, the resistance always increases from 175.9 Ω (1st cycle beginning) to 283.3 Ω (1st cycle end) and to 320.0 Ω (2nd cycle end), which shows that graphene-substrate distance decrease is more pronounced in this case. The shape of the I-V curves for the 2nd cycle for both substrates qualitatively corresponds to a typical shape [15,51], showing no significant inflections.

Simultaneously with the electric current passing in vacuum (I-V measurements), Raman spectra were measured for graphene at each voltage value. Within the sensitivity of the method, no defects were introduced into the graphene structure (the D peak was absent in the Raman spectra). The voltage dependences of ω_G, ω_{2D}, I_{2D}/I_G are presented in Fig. 5 complied with a time-driven scale (dashed lines show the shift

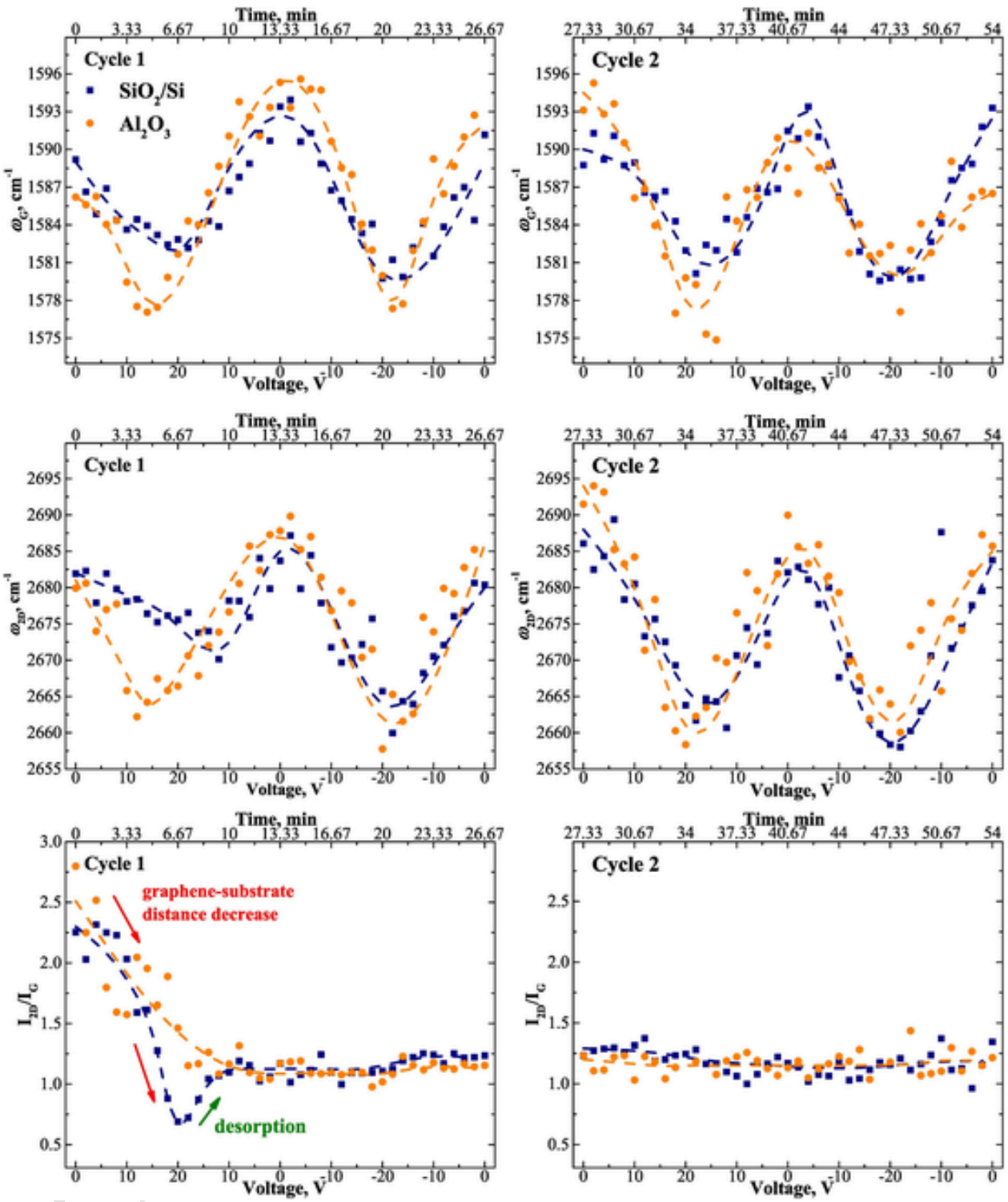

Fig. 5. G and 2D peak positions ω_G, ω_{2D}, and intensity ratio I_{2D}/I_G for graphene on SiO_2/Si and Al_2O_3 depending on voltage during simultaneous I-V measurements in the voltage range from 20 to −20 V.

general direction to improve the clarity of the experimental data). As can be seen from the figure, all peak position dependences have a similar shape for the cases of different substrates; at the same time, the first local minima are reached earlier in the case of the Al_2O_3 substrate, and their shifts are greater by ~4–13 cm^{-1}. The second local minima approximately correspond to each other with regard to voltage and demonstrate shift difference by ~2 cm^{-1}; incidentally, ω_{2D} is greater for the case of the SiO_2/Si substrate in the second cycle. Local maxima have stronger shifts for graphene on Al_2O_3 by 2–10 cm^{-1}, except those in the 2nd cycle for G peak where the opposite is observed (shifts larger by ~2–7 cm^{-1} for graphene on SiO_2/Si substrate). This behaviour itself does not show sufficient patterns for any conclusions to be drawn and requires additional analysis.

The I_{2D}/I_G dependency, associated with the Fermi level position [31], shows a pronounced general decrease with the first voltage increase, followed by saturation, as it was seen in the case of temperature

dependencies in Fig. 2, which along with the increasing resistance in Fig. 4 corresponds to graphene-substrate conformation. Nonetheless, the dependency of I_{2D}/I_G on voltage for graphene on SiO_2/Si also demonstrates a distinctive rise within the 20 → 10 V transition in the 1st cycle. Since it does not repeat afterwards, it is not related to directly voltage-dependent carrier density effects, and therefore we can associate it to acceptor adsorbate removal. As in the case of heat treatment, the resistance is more sensitive to desorption than I_{2D}/I_G within the scale of effects under observation, while the unidirectional graphene-substrate conformation process is most explicitly manifested in the carrier density effects.

While I_{2D}/I_G conceptually agrees with the resistance plots in Fig. 4, it still does not explain ω_G and ω_{2D} voltage dependency behaviour in Fig. 5. In this regard, in order to further distinguish the effects affecting these parameters, it again seems appropriate to plot the 2D-G peak position diagram for points corresponding to zero voltages (to eliminate the influence of electric current and anharmonic effects [22]). Such a diagram is shown in Fig. 6, where points are marked as the following: 1 – the beginning of measurements, 2 – the middle of the first cycle, 3 – the end of the first cycle, 4 – the beginning of the second one, 5 – the middle of the second one, 6 – the end of the measurements (all taken at 0 V). This figure provides additional information about the qualitative changes that occur in the graphene-substrate systems under study after passing electric current accompanied by Joule heating.

In the case of graphene on SiO_2/Si, all changes seen in Fig. 6 align with the *p*-type carrier line. The most pronounced increase 1 → 2 corresponds well to the I_{2D}/I_G decrease in Fig. 5. Other variations along the path 2 → 6 are more specific to 2D-G position diagram only, showing desorption/conformation competition during the treatment; this implies that peak positions might be more informative regarding the charge carrier density effects, provided that other processes that can contribute are excluded [26,27]. The total 1 → 6 excess hole density increase in graphene on SiO_2/Si is $\Delta p \sim 2.3 \times 10^{12}$ cm^{-1} ($\Delta E_F \sim 71$ meV) from peak shift and $\Delta p \sim 5.4 \times 10^{12}$ cm^{-1} ($\Delta E_F \sim 156$ meV) from I_{2D}/I_G decrease. For Al_2O_3-supported graphene, a strong hole density increase occurs on the 1 → 2 transition, which is followed by the diagram points gradually shifting to the area associated with the presence of mechanical strain that corresponds to relative deformation values from 0.068 to 0.076 % [50]. The occurrence of mechanical strain upon further electric current passing through graphene on Al_2O_3 corresponds to a larger degree of graphene-substrate crystal lattice mismatch in this case. At the same time, calculating hole density from peak shifts becomes not possible on the 4 → 6 path; from I_{2D}/I_G decrease, the total 1 → 6 change is of $\Delta p \sim 6.8 \times 10^{12}$ cm^{-1} ($\Delta E_F \sim 213$ meV).

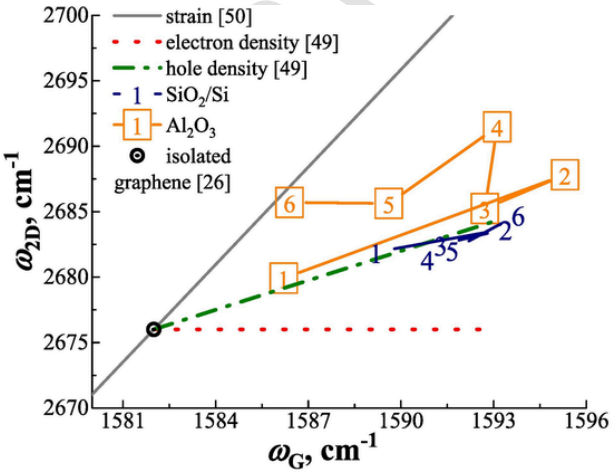

Fig. 6. 2D-G position diagram for graphene on SiO_2/Si and Al_2O_3 before, between and after voltage increases to 20 (−20) V in vacuum; reference point corresponds to isolated graphene.

A decrease of the Fermi level position (effective increase in the hole density) in graphene both after annealing at temperatures of up to 550 °C and after passing an electric current with concomitant heating corresponds to the transition from quasi-suspended (detached) graphene in a minimum energy state to the state of completely supported graphene due to the environment or Joule heating [20]; this evolution explains the deviation from the initial properties of the material close to isolated graphene. The work function for SiO_2 is of 5.00–5.02 eV [52], for α-Al_2O_3 – 5.97–9.66 eV [53], for isolated graphene, it is within 4.48–4.60 eV interval [54,55] (about 4.90 eV when graphene is supported [56]). In this regard, as the graphene-substrate distance decreases, the latter accepts electrons, doping graphene to a *p*-type of electrical conductivity even in the absence of adsorbates, which was reported for both SiO_2/Si [43] and Al_2O_3 [44]. Higher values of the work function for Al_2O_3 correspond to a more significant excess hole density increase in this case.

Charge carrier density and electrical resistance variations in graphene during the processing indicate the presence of oppositely directed processes: a decrease of the graphene-substrate distance (increase of the excess hole density and resistance) and desorption of *p*-type adsorbates from the surface of the material (decrease of the excess hole density and resistance). In terms of the influence on the charge carrier density, estimated from Raman measurements, the conformation of graphene to the substrate dominates, causing a decrease of the Fermi level position, while the resistance, estimated from the electrical measurements, shows a higher sensitivity to desorption. Concerning graphene supported by Al_2O_3, the interaction with which is somewhat weaker as discussed earlier [23,24], the increase of mechanical strain additionally indicates a continued strengthening of interaction energy during the repeated treatments. It should be noted that the heat release when an electric current is passing through graphene is determined by a number of factors, among which is the concentration of defects, and therefore the manifestation of the effect will in principle depend on the initial degree of structural perfection of the material. Therefore, the data from this work can be directly used without adaptation for graphene with an indistinguishable D peak in the Raman spectra.

4. Conclusion

In this work, phonon and electronic properties of graphene on SiO_2/Si and Al_2O_3 were investigated by Raman spectroscopy in the temperature range from room to 550 °C (2 cycles of vacuum annealing) with simultaneous resistance measurements at a direct current of 0.01–1.00 mA, as well as by simultaneous Raman and I-V measurements at voltages from 20 to −20 V (2 cycles of electric current passing/Joule heating).

The removal of air from the vacuum chamber led to the excess hole density decrease $\Delta p \sim 1.8 \times 10^{12}$ cm^{-1} for graphene on SiO_2/Si and $\Delta p \sim 2.4 \times 10^{12}$ cm^{-1} for graphene on Al_2O_3. During the first heating, G and 2D peak positions shifted with the coefficients $\chi_G{}^1 = -0.015$ cm^{-1}/K, $\chi_{2D}{}^1 = -0.042$ cm^{-1}/K for graphene on SiO_2/Si and $\chi_G{}^1 = -0.012$ cm^{-1}/K, $\chi_{2D}{}^1 = -0.030$ cm^{-1}/K for Al_2O_3 case; however, during the following temperature changes the coefficients got stably changed to $\chi_G = -0.026$ cm^{-1}/K, $\chi_{2D} = -0.048$ cm^{-1}/K for graphene on SiO_2/Si and $\chi_G = -0.021$ cm^{-1}/K, $\chi_{2D} = -0.039$ cm^{-1}/K for the Al_2O_3 substrate case. This change is related to graphene-substrate interaction increase due to a transition from quasi-suspended graphene to classically supported one. ω_G, ω_{2D}, I_{2D}/I_G and resistance temperature dependencies showed the evidence of a competition between the *p*-type adsorbate removal from graphene surface (reducing the excess hole density and electrical resistance) and graphene-substrate conformality increase (increasing the excess hole density and resistance). The latter prevailed, with the total average positive

$\Delta p = 3.1 \times 10^{12}$ cm^{-1}, $\Delta R = 149.5$ Ω in the case of SiO_2/Si substrate, and $\Delta p = 5.7 \times 10^{12}$ cm^{-1}, $\Delta R = 16.7$ Ω in the case of Al_2O_3. The resistance temperature coefficients α after reaching a stable R(T) dependence were of $5.1 \cdot 10^{-4}$ K^{-1} and of $5.6 \cdot 10^{-4}$ K^{-1} for graphene on SiO_2/Si and Al_2O_3, respectively.

The I-V curves showed clear steps of competition between graphene-substrate conformation and acceptor adsorbate removal, both stimulated by electric current/Joule heating. The resistance of graphene on SiO_2/Si decreased by 185 Ω after the 1st cycle (domination of desorption) and then increased by 176 Ω at the end of the 2nd cycle (the following prevailing of conformation). For Al_2O_3 substrate, the resistance increased by 107 Ω after the 1st cycle and again by 213 Ω after the 2nd one, showing the permanent dominating graphene-substrate distance decrease during the treatment, after a more significant adsorbate removal back when a vacuum was established in this case. Simultaneous Raman measurements gave a progressive excess hole density increase during the treatment with the total average value $\Delta p \sim 3.9 \times 10^{12}$ cm^{-1} for graphene on SiO_2/Si. For Al_2O_3-supported material, a stronger increase of $\Delta p \sim 6.8 \times 10^{12}$ cm^{-1} occurred, accompanied by emergence of mechanical strain corresponding to average relative deformation value of 0.072 %, which corresponded to a larger degree of graphene-substrate crystal lattice mismatch in this case.

In general, the excess hole density changed unidirectionally and explicitly with the graphene-substrate conformality increase, demonstrating only slight desorption steps, while the resistance and I-V curves had a scaled sensitivity to these effects, and vividly presented their competition. The Al_2O_3 substrate can be used to reduce the desorption barrier, the overall doping, the impact on graphene resistance and on phonon anharmonicity, but should be utilized considering the capacity of strain introduction and stronger doping after longer treatments/stronger interactions. The graphene-substrate conformality effects should be taken into account when performing annealing to remove adsorbates, as well as when designing the material for sensorics applications or passing strong electric currents.

CRediT authorship contribution statement

E.A. Kolesov : Conceptualization, Data curation, Formal analysis, Funding acquisition, Methodology, Project administration, Visualization, Writing – original draft, Writing – review & editing. **M.S. Tivanov :** Supervision, Validation, Resources, Funding acquisition, Data curation, Methodology, Project administration. **O.V. Korolik :** Investigation, Methodology, Project administration, Resources, Validation. **I.A. Svito :** Investigation, Methodology. **A.S. Antonovich :** Formal analysis, Writing – original draft. **Yu. Klishin :** Investigation, Methodology. **D.A. Ghazaryan :** Methodology, Writing – review & editing. **A.V. Arsenin :** Resources, Funding acquisition, Writing – review & editing. **V.S. Volkov :** Resources, Funding acquisition, Writing – review & editing. **O.O. Kapitanova :** Conceptualization, Data curation, Funding acquisition, Methodology, Project administration, Resources, Writing – original draft, Writing – review & editing. **G.N. Panin :** Supervision, Validation, Resources, Funding acquisition, Data curation, Methodology, Project administration.

Declaration of competing interest

The authors declare that they have no known competing financial interests or personal relationships that could have appeared to influence the work reported in this paper.

Data availability

Data will be made available on request.

Acknowledgements

The reported work was funded by Belarusian Republican Foundation for Fundamental Research (project number Φ21PM-140), Russian Foundation for Basic Research (project number 20-57-04010), Russian Science Foundation (project number 23-49-00159), and the Ministry of Science and Higher Education of the Russian Federation (Agreement no. 0714-2020-0002).

References

[1] A.A. Balandin, S. Ghosh, W. Bao, I. Calizo, D. Teweldebrhan, F. Miao, C.N. Lau, Superior thermal conductivity of single-layer graphene, Nano Lett. 8 (2008) 902–907, https://doi.org/10.1021/nl0731872.
[2] K.S. Novoselov, A.K. Geim, S.V. Morozov, D. Jiang, Y. Zhang, S.V. Dubonos, I.V. Grigorieva, A.A. Firsov, Electric field effect in atomically thin carbon films, Science 306 (2004) 666–669, https://doi.org/10.1126/science.1102896.
[3] N. Xin, J. Lourembam, P. Kumaravadivel, A.E. Kazantsev, Z. Wu, C. Mullan, J. Barrier, A.A. Geim, I.V. Grigorieva, A. Mishchenko, A. Principi, V.I. Fal'ko, L.A. Ponomarenko, A.K. Geim, A.I. Berdyugin, Giant magnetoresistance of Dirac plasma in high-mobility graphene, Nature 616 (2023) 270–274, https://doi.org/10.1038/s41586-023-05807-0.
[4] S.B. Kalkan, et al., The effect of adsorbates on the electrical stability of graphene studied by transient photocurrent spectroscopy, Appl. Phys. Lett. 112 (2018) 013103, https://doi.org/10.1063/1.5011454.
[5] G.R. Yazdi, F. Akhtar, I.G. Ivanov, S. Schmidt, I. Shtepliuk, A. Zakharov, T. Iakimov, R. Yakimova, Effect of epitaxial graphene morphology on adsorption of ambient species, Appl. Surf. Sci. 486 (2019) 239–248, https://doi.org/10.1016/j.apsusc.2019.04.247.
[6] S. Ryu, L. Liu, S. Berciaud, Y.-J. Yu, H. Liu, P. Kim, G.W. Flynn, L.E. Brus, Atmospheric oxygen binding and hole doping in deformed graphene on a SiO_2 substrate, Nano Lett. 10 (2010) 4944–4951, https://doi.org/10.1021/nl1029607.
[7] L. Kong, A. Enders, T.S. Rahman, P.A. Dowben, Molecular adsorption on graphene, J. Phys. Condens. Matter 26 (2014) 443001, https://doi.org/10.1088/0953-8984/26/44/443001.
[8] Y. Yang, K. Brenner, R. Murali, The influence of atmosphere on electrical transport in graphene, Carbon 50 (2012) 1727–1733, https://doi.org/10.1016/j.carbon.2011.12.008.
[9] H. Pinto, A. Markevich, Electronic and electrochemical doping of graphene by surface adsorbates, Carbon 5 (2014) 1842–1848, https://doi.org/10.3762/bjnano.5.195.
[10] D.W. Boukhvalov, M.I. Katsnelson, Chemical functionalization of graphene with defects, Nano Lett. 8 (2008) 4373–4379, https://doi.org/10.1021/nl802234n.
[11] Y. Shao, J. Wang, H. Wu, J. Liu, I.A. Aksay, Y. Lin, Graphene based electrochemical sensors and biosensors: a review, Electroanalysis 22 (2010) 1027–1036, https://doi.org/10.1002/elan.200900571.
[12] H. Wang, T. Maiyalagan, X. Wang, Review on recent progress in nitrogen-doped graphene: synthesis, characterization, and its potential applications, ACS Catal. 2 (2012) 781–794, https://doi.org/10.1021/cs200652y.
[13] E.A. Kolesov, M.S. Tivanov, O.V. Korolik, E.Yu. Kataev, Fu Xiao, O.O. Kapitanova, Hak Dong Cho, Tae Won Kang, G.N. Panin, Atmospheric adsorption on pristine and nitrogen-doped graphene: doping-dependent, spatially selective, J. Phys. D. Appl. Phys. 53 (2020) 045302, https://doi.org/10.1088/1361-6463/ab52d9.
[14] E.A. Kolesov, M.S. Tivanov, O.V. Korolik, V.A. Skuratov, O.O. Kapitanova, G.N. Panin, Ion irradiation of supported graphene: defect formation and atmospheric doping, Mater. Sci. Eng. B 284 (2022) 115918, https://doi.org/10.1016/j.mseb.2022.115918.
[15] S. Hertel, F. Kisslinger, J. Jobst, D. Waldmann, M. Krieger, H.B. Weber, Current annealing and electrical breakdown of epitaxial graphene, Appl. Phys. Lett. 98 (2011) 212109, https://doi.org/10.1063/1.3592841.
[16] M. Ishigami, J.H. Chen, W.G. Cullen, M.S. Fuhrer, E.D. Williams, Atomicstructure of graphene on SiO2, Nano Lett. 7 (2007) 1643–1648, https://doi.org/10.1021/nl070613a.
[17] L. Liu, S. Ryu, M.R. Tomasik, E. Stolyarova, N. Jung, M.S. Hybertsen, M.L. Steigerwald, L.E. Brus, G.W. Flynn, Graphene oxidation: thickness-dependent etching and strong chemical doping, Nano Lett. 8 (2008) 1965–1970, https://doi.org/10.1021/nl0808684.
[18] S.M. Song, B.J. Cho, Investigation of interaction between graphene and dielectrics, Nanotechnology 21 (2010) 335706, https://doi.org/10.1088/0957-4484/21/33/335706.
[19] Z. Cheng, Q. Zhou, C. Wang, Q. Li, C. Wang, Y. Fang, Toward intrinsic graphene surfaces: a systematic study on thermal annealing and wet-chemical treatment of SiO2-supported graphene devices, Nano Lett. 11 (2011) 767–771, https://doi.org/10.1021/nl103977d.
[20] K. Kumar, Y.S. Kim, E.H. Yang, The influence of thermal annealing to remove polymeric residue on the electronic doping and morphological characteristics of graphene, Carbon 65 (2013) 35–45, https://doi.org/10.1016/j.carbon.2013.07.088.
[21] H.G. Kim, K. Kihm, W. Lee, G. Lim, S. Cheon, W. Lee, K. Pyun, S. Ko, S. Shin, Effect of graphene-substrate conformity on the in-plane thermal conductivity of supported graphene, Carbon 125 (2017) 39–48, https://doi.org/10.1016/j.carbon.2017.09.033.

[22] E.A. Kolesov, M.S. Tivanov, O.V. Korolik, O.O. Kapitanova, Hak Dong Cho, Tae Won Kang, G.N. Panin, Phonon anharmonicities in supported graphene, Carbon 141 (2019) 190–197, https://doi.org/10.1016/j.carbon.2018.09.020.
[23] E.A. Kolesov, M.S. Tivanov, O.V. Korolik, O.O. Kapitanova, X. Fu, H.D. Cho, T.W. Kang, G.N. Panin, The effect of atmospheric doping on pressure-dependent Raman scattering in supported graphene, Beilstein J. Nanotechnol. 9 (2018) 704–710, https://doi.org/10.3762/bjnano.9.65.
[24] B. Huang, Q. Xu, S.-H. Wei, Theoretical study of corundum as an ideal gate dielectric material for graphene transistors, Phys. Rev. B 84 (2011) 155406, https://doi.org/10.1103/PhysRevB.84.155406.
[25] Y. He, W.F. Chen, W.B. Yu, G. Ouyang, G.W. Yang, Anomalous interface adhesion of graphene membranes, Sci. Rep. 3 (2013) 2660, https://doi.org/10.1038/srep02660.
[26] A.C. Ferrari, D.M. Basko, Raman spectroscopy as a versatile tool for studying the properties of graphene, Nat. Nanotechnol. 8 (2013) 235–246, https://doi.org/10.1038/nnano.2013.46.
[27] J.-B. Wu, M.-L. Lin, X. Cong, H.-N. Liu, P.-H. Tan, Raman spectroscopy of graphene-based materials and its applications in related devices, Chem. Soc. Rev. 47 (2018) 1822–1873, https://doi.org/10.1039/C6CS00915H.
[28] X. Liang, B.A. Sperling, I. Calizo, G. Cheng, C.A. Hacker, Q. Zhang, Y. Obeng, K. Yan, H. Peng, Q. Li, X. Zhu, H. Yuan, A.R. Walker, Z. Liu, L.M. Peng, C.A. Richter, Toward clean and crackless transfer of graphene, ACS Nano 5 (2011) 9144, https://doi.org/10.1021/nn203377t.
[29] L. Gao, G.-X. Ni, Y. Liu, B. Liu, A.H. Castro Neto, K.P. Loh, Face-to-face transfer of wafer-scale graphene films, Nature 505 (2014) 190, https://doi.org/10.1038/nature12763.
[30] M. Her, R. Beams, L. Novotny, Graphene transfer with reduced residue, Phys. Lett. 377 (2013) 1455, https://doi.org/10.1016/j.physleta.2013.04.015.
[31] R. Beams, L.G. Cançado, L. Novotny, Raman characterization of defects and dopants in graphene, J. Phys. Condens. Matter 27 (2015) 083002, https://doi.org/10.1088/0953-8984/27/8/083002.
[32] L. Kong, C. Bjelkevig, S. Gaddam, M. Zhou, Y.H. Lee, G. Han, H. Jeong, N. Wu, Z. Zhang, J. Xiao, P. Dowben, J. Kelber, Graphene/substrate charge transfer characterized by inverse photoelectron spectroscopy, J. Phys. Chem. C 114 (2010) 21618–21624, https://doi.org/10.1021/jp108616h.
[33] A.A. Balandin, Thermal properties of graphene and nanostructured carbon materials, Nat. Mater. 10 (2011) 569–581, https://doi.org/10.1038/nmat3064.
[34] D.L. Nika, A.A. Balandin, Phonons and thermal transport in graphene and graphene-based materials, Rep. Prog. Phys. 80 (2017) 036502, https://doi.org/10.1088/1361-6633/80/3/036502.
[35] K.K. Mishra, S. Ghosh, T.R. Ravindran, S. Amirthapandian, M. Kamruddin, Thermal conductivity and pressure-dependent Raman studies of vertical graphene nanosheets, J. Phys. Chem. C 120 (2016) 25092–25100, https://doi.org/10.1021/acs.jpcc.6b08754.
[36] S. Tian, Y. Yang, Z. Liu, C. Wang, R. Pan, C. Gu, J. Li, Temperature-dependent Raman investigation on suspended graphene: contribution from thermal expansion coefficient mismatch between graphene and substrate, Carbon 104 (2016) 27–32, https://doi.org/10.1016/j.carbon.2016.03.046.
[37] M. Yang, L. Wang, X. Qiao, Y. Liu, Y. Liu, Y. Shi, H. Wu, B. Liang, X. Li, X. Zhao, Temperature dependence of G and D′ phonons in monolayer to few-layer graphene with vacancies, Nanoscale Res. Lett. 15 (2020) 189, https://doi.org/10.1186/s11671-020-03414-w.
[38] I. Calizo, A.A. Balandin, W. Bao, F. Miao, C.N. Lau, Temperature dependence of the Raman spectra of graphene and graphene multilayers, Nano Lett. 7 (2007) 2645–2649, https://doi.org/10.1021/nl071033g.
[39] L.M. Malard, R.L. Moreira, D.C. Elias, F. Plentz, E.S. Alves, M.A. Pimenta, Thermal enhancement of chemical doping in graphene: a Raman spectroscopy study, J. Phys. Condens. Matter 22 (2010) 334202, https://doi.org/10.1088/0953-8984/22/33/334202.
[40] L. Delfour, T.E. Itina, Mechanisms of ultrashort laser-induced fragmentation of metal nanoparticles in liquids: numerical insights, J. Phys. Chem. C 119 (2015) 13893–13900, https://doi.org/10.1021/acs.jpcc.5b02084.
[41] D. Abdula, T. Ozel, K. Kang, D.G. Cahill, M. Shim, Environment-induced effects on the temperature dependence of Raman spectra of single-layer graphene, J. Phys. Chem. C 112 (2008) 20131–20134, https://doi.org/10.1021/jp809501e.
[42] D.J. Late, U. Maitra, L.S. Panchakarla, U.V. Waghmare, C.N.R. Rao, Temperature effects on the Raman spectra of graphenes: dependence on the number of layers and doping, J. Phys. Condens. Matter 23 (2011) 055303, https://doi.org/10.1088/0953-8984/23/5/055303.
[43] M. Adabi, O. Shaforost, S.M. Hanham, L. Hao, N. Klein, Correlation of p-doping in CVD graphene with substrate surface charges, Sci. Rep. 6 (2016) 22858, https://doi.org/10.1038/srep22858.
[44] S. Entani, M. Honda, H. Naramoto, S. Li, S. Sakai, Synchrotron X-ray standing wave characterization of atomic arrangement at interface between transferred graphene and α-Al_2O_3(0001), Surf. Sci. 704 (2021) 121749, https://doi.org/10.1016/j.susc.2020.121749.
[45] D.E. Lee, G. Ahn, S. Ryu, Two-dimensional water diffusion at a graphene–silica interface, J. Am. Chem. Soc. 136 (2014) 6634–6642, https://doi.org/10.1021/ja4121988.
[46] F. Schedin, A.K. Geim, S.V. Morozov, E.W. Hill, P. Blake, M.I. Katsnelson, K.S. Novoselov, Detection of individual gas molecules adsorbed on grapheme, Nat. Mater. 6 (2007) 652–655, https://doi.org/10.1038/nmat1967.
[47] J. Sabio, C. Seoánez, S. Fratini, F. Guinea, A.H. Castro Neto, F. Sols, Electrostatic interactions between graphene layers and their environment, Phys. Rev. B 77 (2008) 195409, https://doi.org/10.1103/PhysRevB.77.195409.
[48] J. Bartolomé, L. Álvarez-Fraga, M.X. Aguilar-Pujol, S. Cortijo, A. Cremades, C. Prieto, A. de Andrés, Grain selective Cu oxidation and anomalous shift of graphene 2D Raman peak in the graphene–Cu system, 2D Mater. 6 (2019) 015023, https://doi.org/10.1088/2053-1583/aaef48.
[49] J.E. Lee, G. Ahn, J. Shim, Y.S. Lee, S. Ryu, Optical separation of mechanical strain from charge doping in graphene, Nat. Commun. 3 (2012) 1024, https://doi.org/10.1038/ncomms2022.
[50] T.M.G. Mohiuddin, A. Lombardo, R.R. Nair, A. Bonetti, G. Savini, R. Jalil, N. Bonini, D.M. Basko, C. Galiotis, N. Marzari, K.S. Novoselov, A.K. Geim, A.C. Ferrari, Uniaxial strain in graphene by Raman spectroscopy: G peak splitting, Grüneisen parameters, and sample orientation, Phys. Rev. B 79 (2009) 205433, https://doi.org/10.1103/PhysRevB.79.205433.
[51] J. Baltazar, C. Henderson, S. Graham, Impact of post-growth thermal annealing and environmental exposure on the unintentional doping of CVD graphene films, 30, 2012 041213, https://doi.org/10.1116/1.4731472.
[52] N.J. Lee, J.W. Yoo, Y.J. Choi, C.J. Kang, D.Y. Jeon, D.C. Kim, S. Seo, H.J. Chung, The interlayer screening effect of graphene sheets investigated by Kelvin probe force microscopy, Appl. Phys. Lett. 95 (2009) 222107, https://doi.org/10.1063/1.3269597.
[53] X.-G. Wang, A. Chaka, M. Scheffler, Effect of the environment on a-Al_2O_3 (0001) surface structures, Phys. Rev. Lett. 84 (2000) 3650–3653, https://doi.org/10.1103/PhysRevLett.84.3650.
[54] P.A. Khomyakov, G. Brocks, V.M. Karpan, J. van den Brink, P.J. Kelly, Doping graphene with metal contacts, Phys. Rev. Lett. 101 (2008) 026803, https://doi.org/10.1103/PhysRevLett.101.026803.
[55] C. Oshima, A. Nagashima, Ultra-thin epitaxial films of graphite and hexagonal boron nitride on solid surfaces, J. Phys. Condens. Matter 9 (1997) 1–20, https://doi.org/10.1088/0953-8984/9/1/004.